Eur. Phys. J. D **4**, 207–218 (1998)

**THE EUROPEAN PHYSICAL JOURNAL D**



# Ionization and energy deposition in metal clusters irradiated by intense lasers

F. Calvayrac[1], A. Domps[1], P.-G. Reinhard[2], E. Suraud[1,a], and C.A. Ullrich[3]

[1] Laboratoire de Physique Quantique, Université Paul Sabatier, 118 Route de Narbonne, 31062 Toulouse Cedex, France
[2] Institut für Theoretische Physik II, Universität Erlangen–Nürnberg, Staudtstr. 7, 91058 Erlangen, Germany
[3] Department of Physics, University of Missouri, Columbia, MO 65211, USA

Received: 2 February 1998 / Revised: 1st June 1998 / Accepted: 18 June 1998

**Abstract.** We study the excitation of metal clusters irradiated by intense laser beams, within the framework of a time dependent density functional approach at fully quantal or semiclassical levels. We focus on ionization processes and energy deposition. It is shown that intense lasers are as efficient as energetic ions to create highly charged clusters, and with comparable deposited excitation energy. We also discuss coupling of electronic to ionic degrees of freedom. We finally consider the importance of accounting for dynamical two-body correlations in the semiclassical approximation and discuss second harmonic generation.

**PACS.** 36.40.Cg Electronic and magnetic properties of clusters – 36.40.Wa Charged clusters – 42.50.Hz Strong-field excitation of optical transitions in quantum systems; multi-photon processes; dynamic Stark shift

## 1 Introduction

The experimental and theoretical investigation of the dynamical properties of simple metallic clusters has been an active field of research for several years now [1,2]. Besides numerous studies devoted to electronic collective modes in the regime of small oscillations [3], which are adequately described within linear response theory [4], there is growing interest in the dynamical behaviour of metal clusters, when strongly excited by collision with an energetic ion or irradiated by an intense laser. This extends current studies of quantum systems under very strong excitations, such as multiphoton processes in atoms [5,6] and small molecules [7] in strong laser pulses (peak intensity $I$ about $10^{13}$ to $10^{16}$ W/cm$^2$, which corresponds to electric field amplitudes of order $E_0 \sim 0.5 - 15\,\mathrm{V}/a_0$), for a recent review see [8]. These strong laser pulses typically have pulse lengths in the range of less than 100 femtoseconds up to several picoseconds, with frequencies $\omega_0$ extending from the infrared to the ultraviolet. With such powerful experimental tools at hand, a wealth of new and sometimes surprising phenomena becomes accessible.

Up to now, most experiments using laser pulses to investigate simple metal clusters have been carried out at relatively moderate laser intensities. There is, however, growing interest in the behaviour of highly charged clusters, which may undergo fragmentation or fission processes [9]. These high charge states may be reached by collisions with highly charged ions [10] or using laser beams. The former method, although efficient, requires a proper (high level) ion source at hand, while lasers are nowadays widely spread experimental devices. Yet, even if used to prepare clusters in high charge states (as in the work of Näher *et al.* [11]), the laser intensities are still often in a regime where ionization proceeds stepwise *via* single-photon processes. Since the pulse lengths used for example in [11] are of the order of nanoseconds, the ionization processes are accompanied by an additional warming of the clusters which may lead to the loss of small fragments already during the charging process. Very recently, however, new experiments with strong femtosecond pulses have been performed which seem to indicate significant differences as compared to the behaviour in the long-pulse regime [12]. More experimental activity of that kind may be expected for the future, and it is thus worthwhile to start theoretical investigations of clusters under the influence of strong laser pulses. Linear response theory ceases to be applicable to such situations, and one needs to recur to a nonlinear approach such as provided within the framework of time-dependent density functional theory (TDDFT) [13,14].

When irradiated by an intense laser, the cluster experiences a short (1 fs to 10–100 fs) and violent electromagnetic pulse. The cluster response is thus primarily (and, first, exclusively) governed by the electron response, which dominates the fs dynamics. The cluster usually loses a sizable fraction of its valence electrons, and undergoes a dipole oscillation (Mie plasmon). The cluster deexcitation

[a] Institut Universitaire de France
e-mail: suraud@irsamc2.ups.tlse.fr

then proceeds by the coupling of electronic to ionic degrees of freedom. Finally, the highly charged cluster fragments, on a time scale of the order of picoseconds. The excitation process evolves, to a totally unknown (and basically not yet investigated) extent, in a non adiabatic way, which makes it hard to justify the Born-Oppenheimer approximation. A proper account for the degree of adiabaticity of the deexcitation phase thus constitutes an important issue. This, however, requires systematic studies, which remain on the edge of today's computational possibilities, although some qualitative insights are already at hand (see below).

In this paper we focus on ionization and energy deposition in clusters irradiated by short and intense laser pulses (intensity $I$ of order $10^{10}$ to $10^{14}$ W/cm$^2$). We show how these quantities can be accessed by means of the TDDFT at various levels of sophistication (fully quantal, semi-classical, possibly complemented by a collision term), possibly including an explicit, non adiabatic, coupling to ionic degrees of freedom. The paper is organized as follows. Section 2 presents the formalism, both in terms of theoretical tools and methods. In Section 3 we give selected results on ionization and energy deposition and transfers. We finally give some conclusions in Section 4.

## 2 Formalism

### 2.1 Electron dynamics

Our description of the valence electron cloud is based on TDDFT [13,14], which has accompanied cluster physics since its early stages [4] and which we have used successfully beyond the linear regime in several previous applications [15–20]. TDDFT may be used at various levels of sophistication, both in terms of the approximation used to describe the exchange-correlation contribution, and in terms of the nature of the description (fully quantal, semiclassical) of the electrons. In this section we recall a few basic formulae necessary for the forthcoming discussions.

#### 2.1.1 The TDKS scheme of DFT

Within TDDFT, the time-dependent density of an $n$-electron system can be obtained, through a set of single-electron wavefunctions $\phi_j(\mathbf{r},t)$ which satisfy the time-dependent Kohn-Sham (TDKS) equation (in atomic units)

$$i\,\frac{\partial}{\partial t}\,\phi_j(\mathbf{r},t) = \left(-\frac{\nabla^2}{2} + v[\rho](\mathbf{r},t)\right)\phi_j(\mathbf{r},t). \qquad (1)$$

The TDKS effective potential $v$ is decomposed into the external potential $v_{ext}(\mathbf{r},t)$, a time-dependent Hartree part and a so-called exchange-correlation ($xc$) potential $v_{xc}\,[\rho](\mathbf{r},t)$:

$$v(\mathbf{r},t) = v_{ext}(\mathbf{r},t) + \int d^3r'\,\frac{\rho(\mathbf{r}',t)}{|\mathbf{r}-\mathbf{r}'|} \;+\; v_{xc}[\rho](\mathbf{r},t), \qquad (2)$$

where the electronic density is given by

$$\rho(\mathbf{r},t) = \sum_{j=1}^{n} |\phi_j(\mathbf{r},t)|^2. \qquad (3)$$

The $xc$ potential is a functional of the density and has to be approximated in practice. The simplest choice, which is used in this work, consists in the TDLDA, defined as $v_{xc}^{TDLDA}(\mathbf{r},t) = \delta E_{xc}^{LDA}/\delta\rho\big|_{\rho=\rho(\mathbf{r},t)}$, where $E_{xc}^{LDA} = \int d^3r\; e_{xc}^{hom}\;(\rho(\mathbf{r}))$ is the static LDA $xc$ energy and $e_{xc}^{hom}(\rho)$ is the $xc$ energy density of the homogeneous electron gas. For $e_{xc}^{hom}$ we use the parametrization of Gunnarsson and Lundqvist [21].

By construction, the TDLDA can be expected to be good only if the time dependence is sufficiently weak. In practice, however, it gives good results even in the case of the rather rapid time dependence of the plasmon response of metal clusters [1,2,4]. We finally mention that it is possible to go beyond the TDLDA in describing dynamical $xc$ effects, for example by including a self-interaction correction (TDSIC) [22]. To our knowledge, the calculations reported in [22] represent to date the most sophisticated attempts to ascertain the relevance of simple TDLDA in the case of metal clusters subject to intense excitations. The results show that differences between TDLDA and TDSIC are minor, with respect to the persistence of gross characteristics of the electronic response, such as ionization patterns and dipole oscillations. The TDLDA method hence represents a realistic first step towards more sophisticated TDDFT methods, and thus clearly suffices for our present exploratory purposes.

#### 2.1.2 Quantal versus semi-classical descriptions

The TDKS scheme (Sect. 2.1.1) can also be formulated in terms of the one-body density operator $\hat{\rho}$:

$$\dot{\hat{\rho}} = \frac{1}{i\hbar}[\hat{h}(\hat{\rho}),\hat{\rho}], \qquad (4)$$

where $\hat{h}$ denotes the single-particle KS Hamiltonian. Besides the quantal approach (4), semi-classical methods can also be worked out. They have actually been used with success in metal cluster dynamics for treating collisions between highly charged ions and metal clusters [18,23]. The Vlasov equation emerges as the semiclassical limit of equation (4). Following the usual rule of thumb, it may be obtained by letting the density operator $\hat{\rho}$ become a phase space density $f(\mathbf{r},\mathbf{p},t)$ and by accordingly replacing the commutator in equation (4) by a classical Poisson bracket. This then leads to the Vlasov equation

$$\frac{\partial f(\mathbf{r},\mathbf{p},t)}{\partial t} + \{f,h\} = 0, \qquad (5)$$

where $h$ is now the classical mean field Hamiltonian depending on the electron density $\varrho(\mathbf{r},t)$, which is computed

as the integral of the phase space distribution over momentum space:

$$\varrho(\mathbf{r},t) = \int d^3p\, f(\mathbf{r},\mathbf{p},t) \tag{6}$$

which represents the semi-classical analogon of equation (3). The semiclassical approximation step leading from equation (4) to equation (5) has nevertheless to be performed with due caution. A discussion of the related expansion in $\hbar$ and the corresponding difficulties can be found in references [24,25].

### 2.1.3 Beyond mean-field

#### *The BUU equation for clusters*

The Vlasov equation represents the basic level of the hierarchy of many-body dynamical equations and is justified in dynamical situations where dissipative effects are not too large. Dynamical two-body correlations come at the next level and allow one to access more dissipative regimes. These correlations run usually at a faster time scale than the mean field motion, and one can thus approximate them by instantaneous two-body collisions. This yields the Vlasov-Boltzmann equation for classical systems. For dense fermion systems, the appropriate statistics has to be built in. This then leads to the so-called Boltzmann-Uehling-Uhlenbeck (BUU) equation which has found widespread application in nuclear physics [26–28]. The resulting BUU equation reads

$$\frac{\partial f}{\partial t} + \{f,h\} = I_{BUU}(f(\mathbf{r},\mathbf{p},t)) \tag{7}$$

with

$$I_{BUU} = \int d\mathbf{p}_2 d\mathbf{p}_3 d\mathbf{p}_4 W(12,34)(f_{12}^{in} f_{34}^{out} - f_{12}^{out} f_{34}^{in}), \tag{8}$$

where $W(12,34)$ is the collision rate

$$W(12,34) = \frac{d\sigma}{d\omega}\delta(\mathbf{p}_1+\mathbf{p}_2-\mathbf{p}_3-\mathbf{p}_4) \times\delta\left(\frac{p_1^2}{2m}+\frac{p_2^2}{2m}-\frac{p_3^2}{2m}-\frac{p_4^2}{2m}\right) \tag{9}$$

expressed as a function of the elementary cross-section $d\sigma/d\omega$. In equation (8), the "in" and "out" label the distribution of particles entering or exiting a two body collision ($12 \leftrightarrow 34$), such that $f_{ij}^{in} = f_i f_j$, $f_{kl}^{out} = (1-f_k)(1-f_l)$, with the short notation $f_i = f(\mathbf{r}_i,\mathbf{p}_i,t)$. This formulation of the outgoing phase space blocking $f_{kl}^{out}$ assumes that the phase space distribution is normalized as $n = \int d^3\mathbf{r}d^3\mathbf{p}f/(2\pi\hbar)^3$ (for a cluster containing $n$ electrons). The Pauli principle shows up explicitly here in these blocking terms, imposing that $f$ should be less than 1, which implies that not more than 1 particle, or 2 with opposite spins, can occupy a phase space cell of volume $(2\pi\hbar)^3$. As known from the theory of Landau liquids, this blocking factor plays a dramatic role for electronic systems [29]. At $T = 0$ K, all the collisions are Pauli blocked and the mean-free path of the electrons becomes infinite. If, at the opposite, the system is hot, or out of equilibrium, phase space opens widely and the effect of two body collisions (apart from asymptotic behavior) can hardly be inferred from formal arguments. Studying the hot electron cascade in which two body events redistribute the energy inside the electron cloud thus requires a numerical approach.

#### *Ingredients of the BUU approach in clusters*

The use of BUU in the present context of the electron response in metal clusters requires some discussion, as it is not (yet) a standard tool of investigation, as for example in nuclear [26] or plasma physics [30]. The key question, beyond a formal justification of the collision integral, which can be inferred from numerous works in nuclear and plasma physics [30], lies in the input cross-section $d\sigma/d\omega$. In the absence of a clear-cut derivation on how to share the effect of the Coulomb interaction between a Hartree, an exchange-correlation and a collision-like two-body contribution, we have chosen to rely on experience gathered in nuclear physics, and, above all, in plasma physics [30] (ruled by the same elementary interaction as the cluster's valence electrons). We chose for $d\sigma/d\omega$ an in-medium (screened) cross-section and keep the LDA $xc$ contribution in the Vlasov part, thus following the local field correction picture of plasma physics, which should ensure no double counting, at least at the phenomenological level we aim at [30]. The screened cross-section is evaluated by inserting a test charge in the system and fitting the screened potential it produces by a Yukawa potential $\propto \exp(-r/d)/r$, which provides a screening length $d = 3a_0$. The screening length is finally translated into a geometrical cross-section $d\sigma/d\omega = \sigma/4\pi$ (computed with the phase shifts method), which will finally enter the BUU collision integral. More details, and a critical discussion on the evaluation of $d\sigma/d\omega$ will be presented elsewhere [31].

#### *More on the double counting problem*

The collision term is derived from a second-order correlation diagram. One thus may suspect that some correlations are possibly double counted when using a collision term in connection with energy-density functionals for the mean-field motion. This question has been much discussed in other fields of physics where similar methods are employed. There is, for example, liquid $^3$He as a dense Fermion system where bubble diagrams play a decisive role similar as for the electron gas. That case had been discussed in [32], and it was worked out that there is no double counting because the collision term (in Markovian approximation) accesses the imaginary part of the effective interaction whereas the mean field uses only the real part. It was, furthermore, pointed out that the collision term should involve the screened interaction as derived from the interaction given in the mean field part. A discussion of the problem for the case of nuclei is found

in [33]. The findings are very similar. But here it was worked out in detail that double counting is no problem only if the collision term is treated in Markovian approximation and that dynamical corrections are to be computed when considering memory effects. In the present treatment, we are using as exploratory tool a simple BUU collision term in Markovian approximation. We thus can assume that there is no double counting of correlations in the procedure, although this point should be checked specifically once for this particular system of electrons in a cluster.

### 2.2 External field: laser excitation and ionic background

The external potential $v_{ext}(\mathbf{r},t)$ in which the electrons move (see Eq. (2)) is made up of two parts:

$$v_{ext}(\mathbf{r},t) = v_{ion}(\mathbf{r}) + E_0\, f(t)\, z\, \sin(\omega_0\, t). \tag{10}$$

The first part, $v_{ion}(\mathbf{r})$, accounts for the Coulomb potential caused by the ionic background of the cluster. The excitations of clusters by femtosecond laser pulses are so rapid that, to a very good approximation, ions can be considered as fixed in the course of the excitation process and during an early stage of the electronic relaxation (typically up to $t \lesssim 100$ fs). In addition, previous investigations of the plasmon response in metal clusters have shown that the details of the ionic structure seem to play only a minor role for the electron dynamics and become less and less important beyond the linear regime [16]. The ionic background of the cluster (nuclei plus core electrons) can thus be safely described in the jellium approximation, as long as one does not consider long time scales at which ionic motion would take place (see Sect. 3.3). Note that we employ the "soft" version [34] of the jellium model, which is equivalent to a folding of the sharp jellium with a pseudopotential characterized by the Ashcroft core radius $r_c$, and allows one to reproduce the experimental plasmon resonance energy in an LDA calculation [35].

Pseudopotentials are required if a detailed description of ionic structures is desired, such as for example when ionic motion is explicitly treated (Sect. 3.3). But here comes the problem that pseudopotentials are usually designed to optimize static structural properties such as the geometry of small systems, and are not particularly good at reproducing dynamical electronic properties like the plasmon peak position. Research on improving pseudopotentials is presently going on [36]. As a preliminary solution we have used a local pseudopotential having the form of the local part of the pseudopotentials from [37] and readjusted the parameters slightly to provide appropriate binding together with plasmon position [38]. We simply take

$$V_{Ps}(\boldsymbol{r}-\boldsymbol{R}) = \sum_{i=1,2} v_i \frac{\mathrm{erf}\left((\boldsymbol{r}-\boldsymbol{R})/\sigma_i\right)}{|\boldsymbol{r}-\boldsymbol{R}|} \tag{11}$$

with

$$\mathrm{erf}(r) = \int_0^r dr'\, \exp\left(\frac{r'^2}{2\sigma_i^2}\right) \tag{12}$$

where $\sigma_2 = 2\sigma_1$, $\sigma_1 = 0.8a_0/(2\sqrt{\ln 2})$, $v_1 = 4.59\sigma_1^2$ and $v_2 = -1.21\sigma_2^2$. This pseudopotential has been successfully tested in connection with the optical response of small sodium clusters, even in the low temperature regime in which the plasmon response is highly fragmented [39]. The accuracy of these calculations is comparable to the one attained using methods of quantum chemistry for small systems [40].

When explicit ionic motion is accounted for, we treat the ions as classical particles described within the standard framework of molecular dynamics. The equations of motion for momentum and position of the $I$-ion then read

$$\frac{d}{dt}P_I = -\nabla_{\mathbf{R}_I}\left[V_{ext}(\mathbf{R}_I,t) - \int d\mathbf{r}\, n(\mathbf{r},t) V_{ps}(|\mathbf{R}_I-\mathbf{r}|) + e^2 \sum_{J\neq I} \frac{1}{|\mathbf{R}_I-\mathbf{R}_J|}\right], \tag{13}$$

$$\frac{d}{dt}R_I = P_I/M_{ion}. \tag{14}$$

They are solved with the standard and robust leap-frog algorithm [41].

The second part of $v_{ext}(\mathbf{r},t)$ (Eq. (10)) is the potential of the laser field. The latter is taken to be polarized along the $z$-axis and has been written in dipole approximation. $E_0$ is the peak field strength and $\omega_0$ the frequency of the laser. The envelope of the pulse $f(t)$ has been chosen either Gaussian for simulating short pulses, or a succession of a (sine or linear) ramp followed by a constant field to simulate longer pulses and to possibly test the impact of a (fainter) steady field.

### 2.3 Observables

We now define the relevant observables for the phenomena we are interested in, namely electron emission and dipole response. The evaluation of electron escape within TDDFT relies on the basic relation

$$N(t) = \int_{\mathcal{V}} d^3r\, \rho(\mathbf{r},t), \tag{15}$$

which associates the number of electrons $N(t)$ remaining in a bound state with the electronic density within a finite volume $\mathcal{V}$ centered around the ionic background. From $N(t)$, one can calculate the total number of escaped electrons as $N_{esc}(t) = N(t=0) - N(t)$ [17]. The dipole moment $d(t)$ with respect to the $z$-axis is evaluated inside the same volume $\mathcal{V}$ [19]:

$$D(t) = \int_{\mathcal{V}} d^3r\, z\, \rho(\mathbf{r},t). \tag{16}$$

From the dipole signal $D(t)$ one can compute the strength function $S(\omega) \propto \mathrm{Im}(\tilde{D}(\omega))$ and the power spectrum $P(\omega) = |\tilde{D}(\omega)|^2$ from the dipole signal in the frequency domain $\tilde{D}(\omega)$. The former gives access to the optical response as measured in the linear regime, and the latter characterizes spectral patterns in the nonlinear domain [19].

An important link with experiment may furthermore be established by calculating probabilities of finding the clusters at a time $t$ in one of the possible charge states $k$ to which they can ionize. In quantal TDKS explicit expressions for the $P^k(t)$ can be obtained in terms of bound-state occupation probabilities $N_j(t)$ associated with the single-particle KS densities $\rho_j$,

$$N_j(t) = \int_{\mathcal{V}} d^3r\, |\phi_j(\mathbf{r},t)|^2 = \int_{\mathcal{V}} d^3r\, \rho_j(\mathbf{r},t). \qquad (17)$$

Since the single-particle KS orbitals have no rigorous physical meaning, one must consider the $P^k[\{\rho_j\}](t)$ defined below only as a reasonable approximation to the exact probabilities. To derive the expressions for the $P^k$'s, we make use of combinatorial considerations which lead us to the following identification ($k = +p, \ldots + n$ for a $\mathrm{Na}_n^{p+}$ cluster):

$$1 = \sum_{k=+p}^{+n} P^k(t) = \prod_{j}^{occ} \left[N_j(t) + (1 - N_j(t))^2\right]^2. \qquad (18)$$

We then work out the right-hand side of equation (18) and rearrange the resulting terms, collecting terms containing $(k-p)$ factors $(1-N_j)$ and $(n-k)$ factors $N_j$. These are then identified with the ionization probabilities $P^k(t)$.

From the above ionization probabilities $P^k$'s one may recover the total number of escaped electrons by simple summation:

$$N_{esc}(t) = \sum_{k=+p}^{+n} kP^k(t), \qquad (19)$$

which thus also appears as the average ionization of the system. In turn, the probability law associated with the set of $P^k$'s allows one to evaluate the standard deviation $\Delta N_{esc}$ around $N_{esc}$ from the variance

$$\Delta N_{esc}^2 = \sum_{k=+p}^{+n} k^2 P^k(t) - \left(\sum_{k=+p}^{+n} kP^k(t)\right)^2. \qquad (20)$$

This provides a more complete, while still compact and rich, account of electron emission properties.

As a final remark, we would like to stress that the robustness of the above defined quantities has been extensively checked in our previous papers (dependence on boundary conditions, role of the finite volume $\mathcal{V}$). We shall not here rediscuss these technical questions and we refer the reader to the proper references on these questions [19,42].

## 2.4 Numerical details

### 2.4.1 Quantal TDKS

The quantal TDKS equation has been solved either in 2D cylindrical or in full 3D geometry (without symmetry restriction). The 2D calculations allow systematic exploratory calculations while the 3D computations provide the most realistic approach. Absorbing boundary conditions have been used throughout. The impact of such boundary conditions has to be carefully checked. This was extensively discussed in [19], and we refer the reader to this reference for details.

In both 2D and 3D cases we use grid techniques for representing the electronic wavefunctions. In 2D we use finite difference formulae for the kinetic energy operator and a Crank-Nicholson scheme for the propagator, for technical details see [19]. The 2D geometry allows the easy treatment of possibly large clusters (up to 100 atoms and more). In such cases, typical computational boxes contain 50–70 (radial direction) $\times$ 200–300 ($z$-direction) grid points, with mesh spacings of order 0.8 $a_0$. The time step is typically taken as $\Delta t = 0.01$ fs.

In the 3D simulations the Laplacian in the kinetic energy and in the Poisson equation is evaluated using fast Fourier transformation. The long-range part of the Coulomb field is handled separately to avoid problems with periodic copies of the fields [43]. The time step employs an interlaced local and kinetic propagation with complex exponentials, *i.e.*

$$\psi_\alpha(t+\delta t) = \exp\left(-i\delta t \hat{T}\right) \exp\left(-i\delta t \hat{V}\right) \psi_\alpha(t) \qquad (21)$$

where the new Kohn-Sham Hamiltonian is recomputed at each full time step. The 3D simulations are best suited for intermediate clusters (10–40 atoms). We typically use $48 \times 48 \times 48$ grid points with a spacing of $0.8\,a_0$, and a time step $\Delta t = 0.0048$ fs.

### 2.4.2 Vlasov and BUU equations

The numerical solution of the Vlasov equation (5) is performed in 3D (without symmetry restriction) using the test-particle method [44]. The one-body distribution $f(\mathbf{r},\, \mathbf{p},\, t)$ is thus projected onto a swarm of $\nu$ numerical test particles as

$$f(\mathbf{r},\mathbf{p},t) \simeq \frac{n}{\nu} \sum_{i=1}^{\nu} g_r(\mathbf{r} - \mathbf{r}_i(t)) g_p(\mathbf{p} - \mathbf{p}_i(t)), \qquad (22)$$

where $g_r$ and $g_p$ are normalized Gaussian functions with width $\sigma_r$ and $\sigma_p$. The Vlasov time propagation for $f$ then follows from classical equations of motion for the $\nu$ test particles, derived from the Hamiltonian [45]

$$h_\nu(\mathbf{r}_i,\mathbf{p}_i) = \frac{\mathbf{p}_i^2}{2m} + v[\rho](\mathbf{r},t) \star g_r(\mathbf{r} - \mathbf{r}_i(t)) \qquad (23)$$

(the symbol "$\star$" stands for the folding operation in coordinate space). It has recently been pointed out [45,46]

that the finite resolution of this numerical method introduces spurious dissipation into the dynamics. This eventually causes the system to evolve towards a Boltzmann equilibrium regardless of the fermionic nature of the system under consideration. Nevertheless, on the short time scales we restrict ourselves when using the Vlasov equation, fermionic stability can be guaranteed by a suitable choice of the numerical parameters $\sigma_r$ and $\nu$. For the computations presented in Section 3.4 a reasonable compromise is $\sigma_r = 1\, a_0$ and $\nu/N = 1500$.

The algorithm used to evaluate the BUU collision term is inherited from the ones developed in nuclear physics [47]. The test particle representation simplifies the horrible integration over phase space by replacing it with a loop over pairs of test particles 1 and 2. The collision rate is governed by the cross-section $\sigma$. The cross-section is translated into a scattering distance $d_\sigma^{phys} = \sqrt{\sigma/\pi}$ that needs to be rescaled to scattering of test particles, which then yields the effective distance $d_\sigma^{eff} = d_\sigma^{phys}\sqrt{n/\nu}$ [47]. The actual sampling then proceeds as follows. Starting from two particles 1 and 2, one previews the distance of closest approach $d_{min}$ of these two particles which will emerge within the coming time step $t \longrightarrow t + \delta t$, and selects those cases which stay within the effective scattering disk, *i.e.* for which $d_{min} \leq d_\sigma^{eff}$. If both criteria are fulfilled, then the two particles collide: $(\mathbf{p}_1, \mathbf{p}_2) \longrightarrow (\mathbf{p}_1', \mathbf{p}_2')$ in accordance with conservation of energy and total momentum. The remaining freedom in the scattering angle is evaluated stochastically. Finally, Pauli blocking is checked by considering target phase space cells for particles 1 and 2. The decision for a successful event is again sampled stochastically, proportional to the amount of open phase space.

It should finally be noted that the BUU collision integral (once Pauli blocking is properly accounted for) leads to a fair stabilization of fermion statistics, as compared to Vlasov. This was expected from the experience in the nuclear case [45]. However, the effect is here more pronounced so that, at least on the time scales we are interested in, the question of loss of statistics can be assumed to be solved in the BUU case.

## 3 Results

### 3.1 Basic electronic response

As a first illustrative example we analyze a typical electronic response to an intense fs laser pulse. We consider a $Na_{93}^+$ cluster, treated in fully quantal TDLDA for the electrons and in the jellium approximation for the ionic background. Calculations have been performed in 2D. The cluster is excited by a trapezoidal laser pulse with 100 fs duration, switched on and off within 10 fs by a linear ramp. The intensity is $I = 10^{11}$ W cm$^{-2}$ and the photon frequency $\hbar\omega \sim 3.1$ eV, about 10% above the Mie resonance for this cluster. Systematic calculations of clusters irradiated with short Gaussian pulses have shown that the cluster response depends crucially on the actual laser frequency [20]. As long as the frequency stays sufficiently far away from the plasmon resonance, the dipole response follows closely the pulse profile and disappears if the laser is switched off. By contrast, if the laser frequency is close to the Mie resonance, one observes damping through electron emission and a true excitation of the plasmon resonance which lasts even after the laser has been switched off. We consider here an example above resonance, but where the resonance comes into play during the process. Results are displayed in Figure 1. For the first 50 fs, the laser pulse is out of resonance and the electronic dipole moment $d(t)$ (upper panel) follows the profile of the laser pulse. Then, however, the amplitude of $d(t)$ starts to increase although the laser intensity does not change. Looking at the middle panel, we see that the number of emitted electrons grows strongly around 50 fs. The remaining cluster acquires a higher charge state, the electron cloud is thus more compressed, and this shifts the plasmon resonance to higher frequencies, *i.e.* closer to the laser frequency. This enhances the response of the system, as seen from the growth of $d(t)$ in the upper panel. The process reaches a peak until the violent electron emission dampens the signal substantially. After the pulse is switched off at $t = 100$ fs and electron emission has come to an end, we find that the remaining electrons continue to perform

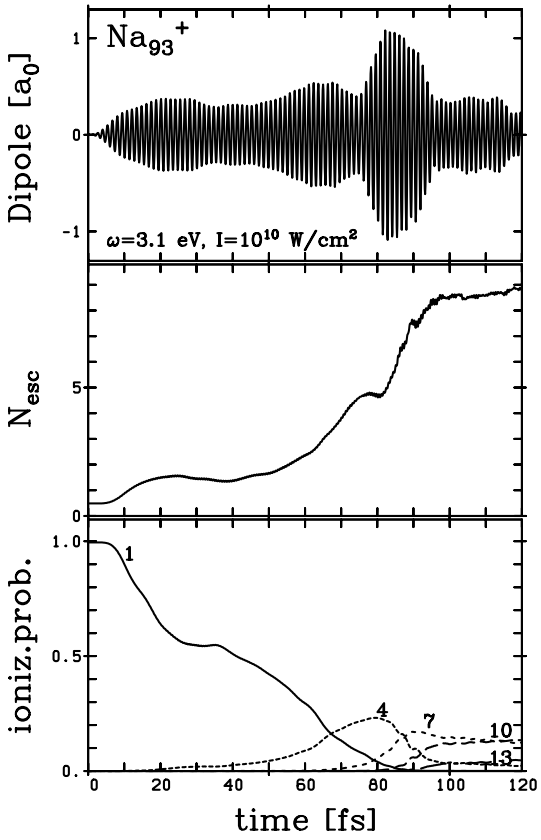


**Fig. 1.** Electronic response of a $Na_{93}^+$ cluster, as a function of time (in fs), to a 100 fs laser pulse of peak intensity $10^{11}$ W/cm$^2$; upper panel: dipole moment along the axis of laser polarization (in $a_0$); middle panel: number of emitted electrons; lower panel: probabilities for some selected charge states, as indicated.

collective oscillations at the actual plasmon frequency of the system, which is slightly above the initial one due to the higher charge state of the final system.

The lower panel of Figure 1 displays the probabilities (Sect. 2.3) of some selected charge states of $Na_{93}$ as a function of time. With the change of $N_{esc}$, the charge state with highest probability changes as well. For example, at 70 fs we have $N_{esc} \sim 3$ and the probability for charge state 4 comes close to its peak, losing weight later on while $N_{esc}$ grows further. The asymptotically dominant charge states lie around 10+. Ionization states higher than this are then rapidly becoming less probable, as we see from the much smaller value for charge state 13+. Note that the number of escaped electrons (middle panel) and the ionization probabilities are formed at basically two time scales. The first (steady) ionization phase leads to a charged cluster resonating with the laser, which leads to a more sudden phase of ionization. This behavior in the second phase is comparable, although involving larger numbers, to the behavior identified in the case of $Na_9^+$ [20].

### 3.2 Collisional versus laser excitation

Laser excitation is not the only way of producing highly charged clusters. A currently much studied, alternative ionization mechanism is provided by collisions with highly charged and fast ions [10]. For velocities of order of the electronic Fermi velocity, these ions deliver a very short and intense electric pulse to the cluster, which again leads to dipole excitation and electron emission. A major difference lies in the time scales, which are below a femtosecond in the case of ion collisions, while fs-laser excitations still typically involve at least some tens of fs. One has to keep in mind that traditional low-intensity lasers take an even longer (nanosecond) span such that slow electron evaporation is accompanied by heating of the electron cloud during the charging process itself [11]. This problem disappears at the fs time scale [12]. We will concentrate here on a comparison between the two fast excitation mechanisms, ion collisions *versus* fs lasers.

Test case is here $Na_9^+$ with jellium approximation for the ionic background. For the ionic excitation we take up an earlier result for a collision with $Ar^{8+}$ at velocity equal to the electronic Fermi velocity and impact parameter $b = 22\,a_0$, for details see [42]. For comparison, we have tuned a fs laser excitation to yield about the same amount of emitted electrons. Actually, we consider a pulse with total duration of 60 fs, switched on and off with a 20 fs sine profile. The pulse has an intensity of $I = 10^{11}\,\mathrm{W/cm^2}$ and frequency $\omega = 2.65\,\mathrm{eV}$, just a bit above the Mie resonance. In Figure 2 we compare these two cases. The middle panel shows that both excitations yield indeed the same asymptotic numbers of escaped electrons. We have also checked the detailed distributions of ionization probabilities, computed according to equation (18). They are generally very similar, leading to comparable (and large) values for the variance equation (20), namely 1.2 particles in the laser case *versus* 1.1 for the ionic excitation. The major difference between the two excitations lies in the time needed

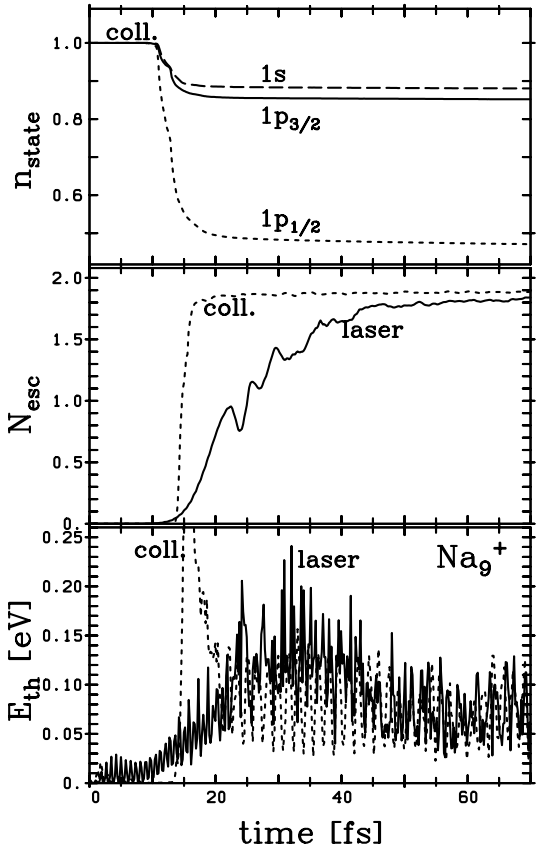


**Fig. 2.** Comparison between an excitation process of a $Na_9{}^+$ cluster by an energetic ion and a laser pulse leading to the same number of emitted electrons (see text for details). The number of emitted electrons $N_{esc}$ (full line) is plotted as a function of time (in fs). In the upper panel are displayed the single particle KS densities $\rho_j$ equation (17) as a function of time (ion collision).

to reach the asymptotic number of emitted electrons. The ionic excitation is extremely fast. The whole excitation energy is transferred in a narrow (sub fs) time-interval around the time of closest approach. This, so to say, sets a rather well-defined clock from which on one can trace clearly the various time scales in the clusters response. We can deduce from the middle panel of Figure 2 that the direct electron emission is a fast process taking only about 2 fs until the asymptotic value is formed. This time is much faster than for the case of laser excitation, where $N_{esc}$ steadily grows over a period of about 30 fs, comparable to the whole duration of the pulse. All in all, however, both times are short compared to the typical ionic time scale (of order 100 fs to 1 ps), which makes both ion collisions and laser excitations suitable trigger mechanisms leading to "clean" fission dynamics.

As the time scales are so different, one may suspect that differences show up in the amount of deposited internal energy. The excitation energy considered here is of thermal nature. We measure this effect by evaluating the difference $E_{th}(t)$ between total collective kinetic energy

and the flow-kinetic energy of the individual particles:

$$E_{th}(t) = \sum_k \int_{\mathcal{V}} \frac{|\mathbf{j}_k(\mathbf{r},t)|^2}{2\rho_k(\mathbf{r},t)} d\mathbf{r} \; - \; \int_{\mathcal{V}} \frac{|\mathbf{j}(\mathbf{r},t)|^2}{2\rho(\mathbf{r},t)} d\mathbf{r}, \qquad (24)$$

where $\mathbf{j}$ and $\rho$ are total local current and density and $\mathbf{j}_k$ and $\rho_k$ are the corresponding quantities for the $k$-th Kohn-Sham orbital. The lower panel of Figure 2 shows this thermal energy for currents along the $z$-axis. There are, of course, differences in the transient regime, due to the different temporal profiles of the excitations. But the asymptotic values agree nicely. Both excitation mechanism, although they seem quite different, deliver at the end the same number of emitted electrons together with the same amount of internal thermalization in these TDLDA simulations.

It is interesting to analyze the mechanism for this thermalization in more detail. The kinetic energy is totally collective if all the particle velocities $\mathbf{j}_k(\mathbf{r},t)/\rho_k(\mathbf{r},t)$ are in phase, and the thermal energy (24) would then disappear. Comparing $N_{esc}$ with $E_{th}$ for the collisional case in Figure 2, we realize that these two processes proceed at the same speed, which suggests that they are closely related. In fact, the reason for the substantial non-collectivity we observe for the electronic motion is that electron emission proceeds at different rates for the different single-particle states, because they are not all bound with the same strength. Consequently, the individual particle velocities get out of phase, and this shows up immediately as thermalization. This is illustrated in the upper panel of Figure 2, which shows the fraction of electrons left bound in the three different single-particle states for the case of ion collision. Obviously, the three states deplete very differently, and this confirms that the thermalization defined here equation (24) is directly related to electron emission, so to speak its counterpart in the electron cloud left behind. This effect is to be distinguished from Landau damping, which becomes effective only for larger clusters above $N \sim 60$ [48].

### 3.3 Coupling electronic to ionic motion

On the time scale of the excitations discussed above, which all stay safely below 100 fs, the ionic background of the cluster can be treated as frozen. But this ceases to apply for time intervals above 100 fs. One soon has to take into account the ionic motion. An example will be given in this subsection.

In addition to the electron dynamics, we now also propagate the classical trajectories for ionic motion equations (13, 14) under influence of the ionic and electronic Coulomb forces, following an approximation as presented in [14]. This approach where ions and electrons are treated on equal footing goes clearly beyond the Born-Oppenheimer approach, which assumes that the electrons follow the ions adiabatically. Diabatic effects are now included in the present treatment.

We consider a $Na_{12}$ cluster irradiated by a Gaussian laser pulse of intensity $I = 5 \times 10^{12}$ Wcm$^{-2}$, with full width at half-maximum of 25 fs, so that at $t = 100$ fs, the excitation is almost over. The laser is linearly polarized along the main diagonal of the principal axis of the cluster, and the photon energy is 6.58 eV, almost twice the plasmon frequency. The plasmon resonance is thus not excited and at the end of the excitation the total electronic dipole moment goes back to its initial value of zero. We have chosen such a high frequency for the laser pulse to have a well-defined (non-collective) excitation of the electronic cloud, with a coupling to the continuum and a direct emission of electrons, although such laser pulses are unlikely to be available in a present-day experimental setup.

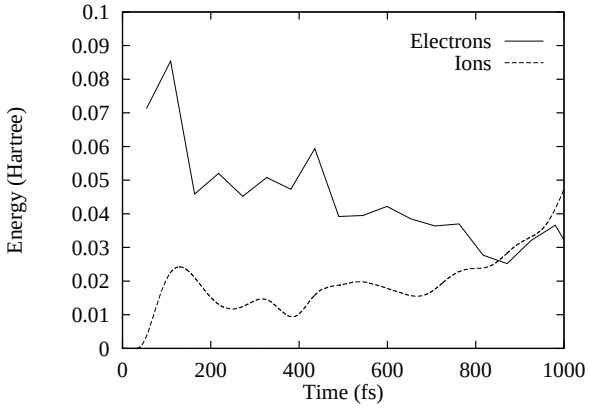


**Fig. 3.** Energy transfer between electrons and ions as a function of time (in fs). The $Na_{12}$ cluster has been excited by a Gaussian laser pulse of peak intensity $I = 5 \times 10^{12}$ W/cm$^2$. The electronic energy is defined in equation (24) and the ionic energy is simply the kinetic energy of ions. Energies are in atomic units.

Approximately 3 electrons are expelled from the cluster at the end of the laser excitation. At $t = 100$ fs we thus have a $Na_{12}^{3+}$ cluster, with an excited electronic cloud which is strongly deformed because of the laser polarization. The ions will thus begin to move since their equilibrium geometry has changed. A reequilibration is here impossible, and the evolution of the ionic dynamics with simultaneous electronic dynamics begins by the emission of two ions followed by roughly two electrons. The remaining cluster is thus approximately a $Na_{10}^{++}$ cluster (mind that TDLDA does not quantify electron numbers), which is still charge-unstable; several fragments are then expelled, which is not enough to stabilize the cluster. Eventually, the cluster is completely destroyed in about 2 ps.

As a first step of the analysis, it is interesting to study the energy transfer between the (initially) excited electron cloud and the ions. The question of final stage fragmentation requires more systematic studies and will be addressed elsewhere [49]. The excitation energies of both electrons and ions are displayed in Figure 3. The electronic component is defined as in equation (24). For the ionic energy we simply take the total ionic kinetic energy, as the ions were initially at rest. The electronic energy, initially high because of the heating by the femtosecond

laser pulse, decreases steadily by energy transfer to the ionic degrees of freedom.

Within the first 100 fs, the ions are found to be almost static, which justifies *a posteriori* the choice of a frozen ionic configuration in all the electronic dynamics computations which we performed before, even in the strongly nonlinear regimes. But after that, the ions start to take their share in the dynamical process at a surprisingly fast time scale, namely within the next 100 fs. The fast coupling between electrons and ions quickly cools the electron cloud, although it was initially very hot. At last, it should be noted that the above described energy transfer is a typical non adiabatic effect which cannot be addressed in conventional Born-Oppenheimer Molecular Dynamics such as Car-Parinello simulations [50], or the calculations of Barnett *et al.* [51]. To our knowledge, the above discussed results constitute the first detailed simulation of the explosion of a metallic cluster induced by a femtosecond laser pulse.

### 3.4 From TDLDA to BUU

As obvious from the results discussed above, irradiation of metal clusters by intense lasers may lead to highly dissipative phenomena, which might call for a description of electrons beyond the mere mean-field. The BUU equation presented in Section 2.1.3 constitutes a first attempt to go beyond mean-field. It is thus interesting to compare a Vlasov and a BUU description of the excitation of a metal cluster by an intense laser.

Figure 4 represents the dipole signal, as calculated in Vlasov and BUU, obtained when applying a Gaussian laser pulse with peak intensity $10^{12}$ W/cm$^2$ to $Na_9^+$. The laser frequency matches the plasmon resonance and the width is 20 fs. The peak intensity occurs at $t = 30$ fs. The amplitude of the BUU case is of course lower than the amplitude of the Vlasov case, because of the larger dissipation in BUU. The difference is well visible in the relaxation stage: once the laser is off, the dipole signal quickly relaxes if two body collisions are implemented. But we can also see large differences in the excitation stage, *i.e.* while the amplitudes grows. Less energy is transfered by the laser into the plasmon, the difference getting converted into thermal energy of the electrons. Two body collisions indeed play their role to redistribute energy into local, non collective motion.

It is instructive to perform a more detailed analysis of the plasmon damping in Figure 4 in order to access time scales. As a first estimate, as read from Figure 4, we compare plasmon signals from $t \sim 35$ fs on. A Fourier analysis of both signals easily allows us to obtain a plasmon linewidth $\Gamma$, from the FHWM. We respectively find $\Gamma_{BUU} \sim 0.2$ eV and $\Gamma_{Vla.} \simeq 0.06$ eV, which respectively leads to lifetimes of order $\tau_{BUU} \sim 3$ fs and $\tau_{Vla.} \sim 10$ fs. The latter lifetime $\tau_{Vla.}$ provides a measure of Landau damping. The BUU can be interpreted in the light of results from Landau Fermi liquid theory [29]: for a quasiparticle with energy $\epsilon$ in a Fermi sea with temperature $T$,

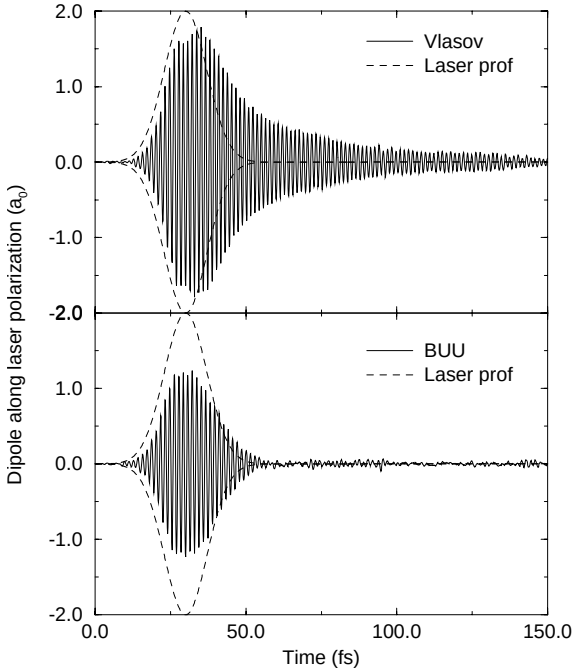


**Fig. 4.** Comparison between an excitation process of a $Na_9^+$ cluster by a Gaussian laser pulse of peak intensity $I = 10^{12}$ W/cm$^2$, as calculated in Vlasov (upper panel) and in BUU (lower panel). The dipole moment (in $a_0$) along laser polarization is plotted as a function of time (in fs). The envelop of the laser profile is also plotted (dashed lines).

we expect a collision time

$$\frac{1}{\tau_{ee}} = K \frac{\pi^2 T^2 + (\epsilon - \epsilon_F)^2}{1 + exp(-(\epsilon - \epsilon_F)/T)} \cdot \qquad (25)$$

The prefactor $K$ has been recently measured in bulk Ag [52,53], with values in reasonable agreement with the RPA prediction $K^{-1} = a\, n^{5/6}$ [29], where $a = 16\pi^{1/6} 3^{5/6} \hbar^4 / (e^2 m^3)^{1/2}$. Applying this formula to sodium, we obtain at Fermi level ($\epsilon = \epsilon_F$) $1/\tau_{ee} = 0.6\, T^2$. The temperature entering the above evaluations can be accessed in our case by fitting the single-particle electronic occupation numbers to a Fermi distribution, which provides a measure of the system temperature [54]. Such a procedure leads to an electronic temperature of order 1.2–1.3 eV for times beyond 50 fs. Inserting this value in the above formula we obtain $\tau_{ee} \sim 1$–$1.2$ fs, which, at the rough qualitative level at which we presently stay, is compatible with our above estimate.

The above estimate of cluster temperature also provides interesting information on the further behavior of electrons. As the heating process in BUU is more efficient than in Vlasov, the cluster keeps emitting electrons after the laser has been switched off because it is now very hot: the temperature of 1.2–1.3 eV corresponds to almost half the initial Fermi level at final time. The electron evaporation rate, around 0.007 electron per femtosecond, has a magnitude consistent with the prediction of the Weisskopf formula [55]. This confirms the thermal interpretation for this retarded electron emission.

It remains to see whether this modified energy balance will show up in the coupling to ionic motion as discussed in Section 3.3, or whether it would interfere with excitation processes involving a "comparable" time scale as, *e.g.*, laser pulses of 20–50 fs duration.

### 3.5 Second harmonic generation

Laser excitation carries a given frequency and the linear response explores the spectral properties of a system at this frequency. The dipole response to a harmonic laser field is then $D(t) = \alpha_1 E_0 \exp(-i\omega t)$ where $E_0$ is the laser field strength, $\omega$ the frequency, and $\alpha_1(\omega)$ the coefficient of linear polarizability. Nonlinear effects can couple to sidebands of multiple frequencies such that one deals with the generalized response

$$D(t) = \alpha_1 E_0 e^{-i\omega t} + \alpha_2 E_0^2 e^{-i2\omega t} + \alpha_3 E_0^3 e^{-i3\omega t} + ... \quad (26)$$

The coupling decreases with increasing multiplicity and the first sideband to look at lies at double frequency, known as second harmonic generation (SHG). SHG with particularly suited crystals is a standard tool for frequency doubling of laser beams. But SHG is also often used as a means to analyze the nonlinear response of a system. In this spirit, it has also been applied to large metal clusters attached to a surface, see *e.g.* [56]. Amongst the many aspects of SHG, one of the first questions is under which conditions one may obtain the largest response. Analytical estimates within an oscillator model plus small anharmonic perturbation suggest that the resonance frequency, the Mie plasmon frequency $\omega_{pl}$, should be involved at some end of the process, either by shining at the cluster with $\omega = \omega_{pl}$ (SHG "out of the resonance"), or by placing the second harmonics at $2\omega = \omega_{pl}$ (SHG "into resonance"). We have investigated both options for the test case $Na_9^+$ in the ionic 144 configuration from the cylindrically averaged pseudopotential scheme (CAPS) [57]. The 144 means that the ions are arranged as one single ion followed by a ring of four ions and continued by a second ring of four ions where the two rings are rotated by 45° relative to each other to minimize the Coulomb energy. This ionic structure involves a slight asymmetry with an octupole moment of $\beta_3 = -0.2$. This turns out to be just sufficient for our purposes, since SHG only occurs if inversion symmetry is broken.

We apply a laser pulse of 60 fs duration, switched by a ramp of 6 fs at the beginning and the end. The induced dipole moment $D(t)$ is recorded and Fourier transformed to $\tilde{D}(\omega)$ at the end of the process. The power spectrum $\mathcal{P}(\omega) = |\tilde{D}(\omega)|^2$ thus obtained is shown in Figure 5. The lowest panel represents the case of SHG "into resonance", where the cluster is excited at approximately half the resonance frequency. One sees a nice and clean SHG signal far above background. The shape of the SHG peak is somewhat twisted due to a slight (and deliberate) mismatch of the frequencies. The $2\omega$ and the $\omega_{pl}$ components both fight for their share, and what we see here is the compromise thus found. The middle panel stands for the case of SHG

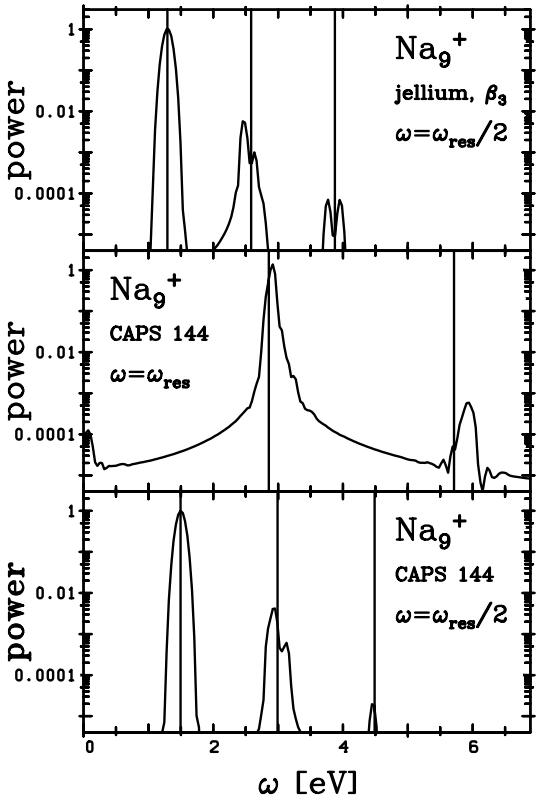


**Fig. 5.** Dipole power spectra for $Na_9^+$ from excitation with a laser pulse over 60 fs. The two lower panels are computed with detailed ionic background in the CAPS 144 configuration [57] and a jellium background with the same octupole deformation $\beta_3 = -0.2$ was used in the upper panel. Two laser frequencies $\omega$ are employed as indicated ($\omega_{res}$ is the Mie plasmon frequency for the given model).

"out of the resonance". There is again a nicely visible SHG signal and again a perturbation of the peak, here probably due to interference with the volume plasmon which resides near this frequency. However, the background is larger than in the previous case. This is due to the fact that the system in resonance reacts more strongly and the emerging larger amplitude causes a much more dramatic perturbation of the system. Comparison shows that SHG works efficiently both ways as expected from the analytical estimate. But the case of SHG "into resonance" seems to be a bit more preferable because there is less perturbation of the cluster (which, in turn, allows one to use higher intensities).

The test case has symmetry breaking and includes ionic structure. It is interesting to check the impact of ionic structure on the emerging SHG. To this end, we have recomputed the SHG "into resonance" using a jellium background with exactly the same deformation parameters as the 144 CAPS configuration. The result is shown in the upper panel of Figure 5. It looks quite similar to the result in the lowest panel (mind that the CAPS Mie plasmon is slightly blue shifted as compared to the jellium value, which is a well-known short coming of CAPS [38]). This demonstrates that the symmetry-breaking, parametrized

here in terms of the octupole moment $\beta_3$, is the crucial ingredient for the SHG. In addition, it is to be remarked that free clusters have usually rather small $\beta_3$. The experiments on SHG have actually been done for clusters attached to a surface [56], which induces a much larger symmetry breaking. We have checked that aspect by considering also a value of $\beta_3 = 0.4$ as found by recent calculations of $Na_8$ on a surface of NaCl [58,59]. This enhances the SHG by three orders of magnitude, such that the SHG peak (in the case "into resonance") is even higher than the peak at the laser frequency. Thus far we can qualitatively reproduce the experimental findings. But a detailed comparison is hindered by the fact the the measurements of reference [56] are done for huge clusters ($N \sim 10^6$) to get stronger signals. Nonetheless, the above exploratory example demonstrates that TDLDA is the appropriate tool also for the study of the SHG. This motivates a more systematic survey of of SHG, which is planned for the near future.

## 4 Conclusions and perspectives

We have presented simulations of the electronic and ionic response in a metal cluster irradiated by an intense laser beam. Since we consider strong perturbations, we have used methods based on a full time-dependent description of electronic degrees of freedom, by means of the TDDFT at various levels of approximations. The coupling to ionic degrees of freedom has also been accounted for, in a non adiabatic way. The models developed allow one to access a wealth of new interesting phenomena occurring in metal clusters irradiated by intense laser beams with typical intensities below $10^{15}$ W/cm$^2$.

We have found that the electronic response, which sensitively depends on the choice of the laser frequency relative to the frequency of the Mie plasmon, is characterized by a collective oscillation and (possibly strong) emission. A comparison to charging by means of collisions with energetic ions has shown that comparable ionization states may easily be attained with moderately intense lasers. The study of the coupling of electronic to ionic degrees of freedom has furthermore revealed that this coupling takes place on a very short time scales, thus raising doubts on the possible relevance of adiabatic, Born-Oppenheimer-based approaches in connection with energetic laser excitation. Furthermore, extension of our methods to incorporate dynamical two body collisions by means of a collision integral of Boltzmann type has shown that such a mechanism does significantly change the energy transfers in the course of the excitation of the cluster, which might, in turn, influence the ensuing evolution of the system, for example towards fission or fragmentation. Finally, we have investigated second-harmonic generation from fs laser pulses. This requires some reflection-symmetry breaking in the cluster ground state to operate at all. Optimum efficiciency is achieved if the second harmonics coincides with the plasmon resonance.

The authors thank the French-German exchange program PROCOPE number 95073 and Institut Universitaire de France for financial support during the realization of this work. IDRIS is also thanked for extended computational facilities.

## References

1. W. de Heer, Rev. Mod. Phys. **65**, 611 (1993).
2. M. Brack, Rev. Mod. Phys. **65**, 677 (1993).
3. G.F. Bertsch, R. Broglia, *Oscillations in finite quantum systems* (Cambridge Univ. Press, 1994).
4. W. Ekardt, Phys. Rev. Lett. **52**, 1925 (1984); Phys. Rev. B **31**, 6360 (1985); Phys. Rev. B **32**, 1961 (1985).
5. K.C. Kulander, Phys. Rev. A **36**, 2726 (1987).
6. *Atoms in intense fields*, edited by M. Gavrila (Academic Press, San Diego, 1992).
7. *Molecules in laser fields*, edited by A.D. Bandrauk (Marcel Dekker, New-York, 1993).
8. M. Protopapas, C.H. Keitel, P.L. Knight, Rep. Prog. Phys. **60**, 389 (1997) and references therein.
9. U. Näher, S. Bjornholm, S. Frauendorf, F. Garcias, C. Guet, Phys. Rep. **285**, 245 (1997).
10. F. Chandezon, C. Guet, B.A. Huber, D. Jalabert, M. Maurel, E. Monnand, C. Ristori, J.C. Rocco, Phys. Rev. Lett. **74**, 3784 (1995).
11. U. Näher, H. Göhlich, T. Lange, T.P. Martin, Phys. Rev. Lett. **68**, 3416 (1992); U. Näher, S. Frank, N. Malinowski, U. Zimmermann, T.P. Martin, Z. Phys. D **31**, 191 (1994).
12. R. Schlipper, R. Kusche, B. von Issendorff, H. Haberland, Phys. Rev. Lett. **80**, 1194 (1998).
13. E.K.U. Gross, C.A. Ullrich, U.J. Gossmann, in *Density Functional Theory*, edited by E.K.U. Gross, R.M. Dreizler, NATO ASI series B337 (Plenum Press, New York, 1994).
14. E.K.U. Gross, J.F. Dobson, M. Petersilka, in *Topics in Current Chemistry*, edited by R.F. Nalewajski (Springer, 1996).
15. C.A. Ullrich, S. Erhard, E.K.U. Gross, in *Super-Intense Laser-Atom Physics IV*, edited by H.G. Muller, M.V. Fedorov (Kluwer, Dordrecht, 1996); C.A. Ullrich, E.K.U. Gross, Comments At. Mol. Phys. **33**, 211 (1997).
16. F. Calvayrac, P.-G. Reinhard, E. Suraud, Phys. Rev. B **52**, R17056 (1995).
17. C.A. Ullrich, P.-G. Reinhard, E. Suraud, Phys. Rev. A **57**, 1938 (1998).
18. L. Féret, E. Suraud, F. Calvayrac, P.-G. Reinhard, J. Phys. B: At. Mol. Opt. Phys. **29**, 4477 (1996).
19. F. Calvayrac, P.-G. Reinhard, E. Suraud, Ann. Phys. (N.Y.) **255**, 125 (1997).
20. C.A. Ullrich, P.-G. Reinhard, E. Suraud, J. Phys. B: At. Mol. Opt. Phys. **30**, 5043 (1997).
21. O. Gunnarsson, B.I. Lundqvist, Phys. Rev. B **13**, 4274 (1976).
22. C.A. Ullrich, P.-G. Reinhard, E. Suraud, J. Phys. B: At. Mol. Opt. Phys. **31**, 1871 (1998).
23. M. Gross, C. Guet, Z. Phys. D **33**, 289 (1995).
24. P. L'Eplattenier, E. Suraud, P.-G. Reinhard, Ann. Phys. (N.Y.) **224**, 426 (1995).
25. A. Domps, P. L'Eplattenier, P.-G. Reinhard, E. Suraud, Ann. Phys. (Leipzig) **6**, 455 (1997).
26. G.F. Bertsch, S. Das Gupta, Phys. Rep. **160**, 190 (1988).

27. A. Bonasera, F. Gulminelli, J. Molitoris, Phys. Rep. **243**, 1 (1994).
28. Y. Abe, S. Ayik, P.-G. Reinhard, E. Suraud, Phys. Rep. **275**, 49 (1996).
29. D. Pines, P. Nozières, *The theory of Quantum Liquids* (W.A. Benjamin, New York, 1966).
30. S. Ichimaru, H. Iyetomi, S. Tanaka, Phys. Rep. **149**, 91 (1987).
31. A. Domps, P.-G. Reinhard, E. Suraud, in preparation.
32. J.W. Serene, D. Rainer, Phys. Rep. **101**, 221 (1983).
33. K. Gütter, K. Wagner, P.-G. Reinhard, C. Toepffer, Ann. Phys. (N.Y.) **225**, 339 (1993).
34. B. Montag, P.-G. Reinhard, J. Meyer, Z. Phys. D **32**, 125 (1994).
35. P.-G. Reinhard, O. Genzken, M. Brack, Ann. Phys. (Leipzig) **5**, 1 (1996).
36. M. Brack, S. Kümmel (private communication).
37. G.B. Bachelet, D.R. Hamann, M. Schlüter, Phys. Rev. B **26**, 4199 (1982).
38. F. Calvayrac, P.-G. Reinhard, E. Suraud, J. Phys. B: At. Mol. Opt. Phys., **31**, 1367 (1998).
39. T. Reiners, C. Ellert, M. Schmidt, H. Haberland, Phys. Rev. Lett. **74**, 1558 (1995).
40. V. Bonačić-Koutecký, P. Fantucci, J. Koutecký, Chem. Rev. **91**, 1035 (1991).
41. L. Verlet, Phys. Rev. **159**, 98 (1967).
42. P.-G. Reinhard, E. Suraud, C.A. Ullrich, Eur. Phys. J. D **1**, 303 (1998).
43. G. Lauritsch, P.-G. Reinhard, Int. J. Mod. Phys. C **5**, 65 (1994).
44. W.G. Hoover, *Computational statistical mechanics* (Elsevier, 1991).
45. P.-G. Reinhard, E. Suraud, Ann. Phys. (N.Y.) **239**, 216 (1995).
46. A. Domps, A.S. Krepper, V. Savalli, P.-G. Reinhard, E. Suraud, Ann. Phys. (Leipzig) **6**, 468 (1997).
47. G. Welke, R. Malfliet, Ch. Grégoire, M. Praksah, E. Suraud, Phys. Rev. C **40**, 2611 (1989).
48. J. Babst, P.-G. Reinhard, Z. Phys. D **42**, 209 (1997).
49. F. Calvayrac, P.-G. Reinhard, E. Suraud, J. Phys. B (in press, 1998).
50. R. Car, M. Parinello, Phys. Rev. Lett. **55**, 2471 (1985).
51. R.N. Barnett, U. Landman, A. Nitzan, G. Rajagopal, J. Chem. Phys. **94**, 608 (1991).
52. M. Wolf *et al.*, Phys. Bl. **54**, 154 (1998).
53. R.H.M. Groeneveld *et al.*, Phys. Rev. B **51**, 11433 (1995).
54. A. Domps, P.-G. Reinhard, E. Suraud, Ann. Phys. (N.Y.) **260**, 171 (1997).
55. V. Weisskopf, Phys. Rev. **52**, 295 (1937).
56. A. Assion, B. Lang, M. Simon, S. Voll, F. Traeger, G. Gerber, Chem. Phys. Lett. (to appear, 1998).
57. B. Montag, P.-G. Reinhard, Z. Phys. D **33**, 265 (1995).
58. C. Kohl, P.-G. Reinhard, Z. Phys. D **39**, 605 (1997).
59. C. Kohl, F. Calvayrac, P.-G. Reinhard, E. Suraud, Surf. Sci. **405**, 74 (1998).